Microscopic and spectroscopic evaluation of SPS sintered aluminium-graphene (Al-Gr) nanocomposites

Vipin Jain*, Anil Kumar, Ajay Dhar

CSIR-National Physical Laboratory, Dr. K.S. Krishnan Marg, New Delhi, 110012, India

*Corresponding author, E-mail: vipin@nplindia.org; Tel: (+91)114-5609421/9456

Received: 29 March 2016, Revised: 28 September 2016 and Accepted: 20 December 2016

DOI: 10.5185/amp.2017/303
www.vbripress.com/amp

Abstract

Graphene possesses excellent properties such as, high Young's modulus (1 TPa), high fracture strength (~125 GPa) and extreme thermal conductivity (~5000 W/m/K), therefore, can serve as an ideal reinforcement material for the metal based *High Tech* structural nanocomposites. In the present work, a novel chemical synthesis method has been adopted for the *in-situ* synthesis of aluminium-graphene (Al-Gr) nanocomposite powders with varying compositions using graphene oxide (GO) as the precursor. The pure aluminium powder was initially cryomilled to refine the crystallite size. Subsequently, Al-reduced graphene (Al-Gr) nanocomposite powders were synthesized employing different volume proportions of GO (referred as 0.5, 2, 4, and 6 ml) dispersed in deionized water. The synthesized nanocomposite powders were ball milled followed by consolidation using spark plasma sintering under the optimized conditions. The nanocomposite powder as well as SPSed samples were characterized using X-ray diffraction (XRD), Raman Spectroscopy and electron microscopy. Scanning electron microscopy (SEM) studies of nanocomposite powders have depicted wrinkled structure typical of reduced graphene. Raman spectra have shown regular D, G, 2D and D+G bands and a modulated 2D peak having intensity significantly less than the G peak was observed for the nanocomposite powders confirming multilayered graphene is synthesized. The graphene wrinkles were determined in the size of 100 nm or more. Microhardness of SPS sintered nanocomposites is found progressively increased with the increasing content of reduced graphene with up to 58% improvement over pure Al was observed for the maximized GO content depicting potential for energy efficient high strength applications. The synthesized Al-graphene nanocomposites are novel in terms of an innovative, indigenously developed and scalable to bulk synthesis approach based on *in-situ* chemical synthesis route adopted.

Keywords: Graphene, nanocomposites, raman spectroscopy, SPS, electron microscopy.

Introduction

Research on graphene reinforced-metal matrix nanocomposites has been accelerated since 2010 to meet the demand of improved mechanical properties **[1-3]** which could be exploited for energy efficient *High Tech* automotive applications due to light weight. Other advanced energy applications of these nanocomposites include for photovoltaic **[4]**, hydrogen storage **[5]**, lithium ion batteries **[6, 7]** etc. Smart technologies and novel synthesis processes are the research areas for the development of these nanocomposites for either achieving improved energy efficiency of vehicles through light weighing or finding alternate sources of energy production. Graphene (Gr) has emerged as the ideal reinforcement material for the synthesis of metal based structural nanocomposites with improved mechanical properties for achieving improved energy efficiency of vehicles. This has been due to the excellent mechanical properties of graphene (a high fracture strength of the order of 125 GPa and high Young's modulus of the order of 1 TPa etc. **[2-3]**. The two dimensional sheet like structure with a high aspect ratio and larger surface area compared to CNTs could enable achieving enhanced mechanical and physical properties of graphene reinforced metal matrix structural nanocomposites. The overall enhancement in the mechanical properties of Gr-reinforced nanocomposites further depends on the synthesis method used for the dispersion of Gr in the metallic powder and the consolidation route adopted etc.

Several methods, such as flake powder metallurgy **[3,8]**, pulse reverse electrodeposition (PRED) **[9]**, molecular level mixing **[10]**, solvothermal synthesis **[11]**, ultrasound assisted preparation **[12]** etc. have been adopted for the synthesis of graphene reinforced metal (Al/Cu/Ag) matrix nanocomposites. The flake powder metallurgy route adopted by Wang *et al* **[3]**

followed by sintering in argon and hot deformation subsequently, has reported 62% enhancement in tensile strength with 0.3 wt% addition of graphene nanosheets (GNSs) over unreinforced aluminium matrix. The detailed surface modification process for flake powder metallurgy has been reported by Jiang *et al* **[8]**. The PRED electrodeposited Cu-Gr nanocomposite foils delivered 96% increase in hardness compared to pure copper **[9]**. Hwang *et al* **[10]** have reported molecular level mixing of copper-graphene nanocomposites followed by spark plasma sintering (SPS) enabling up to 1.8 times (or 80%) improvement in yield strength over pure copper, whereas, Jun *et al* **[11]** have synthesized silver-graphene nanocomposite foils using the solvothermal synthesis route for the improvement in mechanical properties. Graphene properties, synthesis routes, and applications have been recently reviewed recently by A. Tiwari **[13]**.

In the present work, a novel processing route for the *in-situ* chemical synthesis of aluminum-reduced graphene (Al-Gr) nanocomposites is adopted using graphene oxide (GO) as the precursor. Using this novel process, Al-Gr nanocomposites with varying proportions of GO are synthesized followed by ball milling for the homogenous mixing. Subsequently, the nanocomposite powders are consolidated using spark plasma sintering (SPS). The pure aluminum powder was initially cryomilled in liquid nitrogen to reduce the crystallite size and then subjected to *in-situ* chemical synthesis. The synthesized Al-Gr nanocomposites are novel in terms of an innovative, indigenously developed and scalable for bulk synthesis approach for the development of energy efficient high strength Al-Gr nanocomposites. Structure-property correlation of the synthesized nanocomposites has been conducted using electron microscopy (SEM/TEM), Raman spectroscopy, and mechanical behaviour evaluation etc.

Experimental

Materials and in-situ chemical synthesis

Pure aluminium powder (>99.5% purity) procured from a commercial supplier was used as the matrix material. Graphene oxide (GO) used as precursor for this study, was prepared in-house. For this purpose, graphite powder (~99.9% C) was used as the starting materials to obtain GO using a modified Hummers method **[4, 14]**. Hydrazine hydrate ($NH_2NH_2.2H_2O$, 99.9% pure) was used as a reducing agent. As the initial processing step, pure aluminium powder was cryomilled in a cryogenic attritor using liquid nitrogen as the dispersion media employing steel balls of 5 mm dia keeping balls to powder weight ratio (BPR) of 20:1 and milling time as 2 h. Dispersed GO by volume (0.5, 2, 4 and 6 ml) was added with pure aluminium powder (10 g) in deionized water and stirred on a hot plate at ~70 °C. Subsequently hydrazine hydrate (10 ml) was added as the reducing agent (to reduce GO to reduced graphene) and stirring was conducted up to 2 h. **Table 1** shows different compositions and sample IDs used in this study to prepare the Al-Gr nanocomposite powder. The Al-Gr nanocomposite powders ware dried in an oven for half an hour and ball milled under optimized conditions [BPR-15:1, speed-200/400 (vial/platen), dia of steel balls-5 mm, milling time: 30 min].

Table 1. Aluminium-reduced graphene (Al-Gr) nanocomposites for *in-situ* chemical synthesis.

S. No.	Specimen ID	Composition (by weight/volume)	
		Pure Al powder (g)	Dispersed Graphene Oxide (GO) (ml)
1.	Pure Al	10	0
2.	Al- 0.5 Gr	10	0.5
3.	Al-2 Gr	10	2
4.	Al-4 Gr	10	4
5.	Al-6 Gr	10	6

Consolidation using spark plasma sintering (SPS)

The ball milled powders were consolidated on spark plasma sintering (SPS) facility (*SPS Syntex, Japan*). Graphite dies were used for the consolidation of the powder samples. Initial optimization trials were conducted on Al-0.5 Gr composite powder for which the SPS parameters used were load: 8.5 kN, heating rate: 50 °C/min, heating time: 5 min and sintering temperature: 450, 500, and 550 °C. Subsequently, rest of the samples were sintered at the temperature of 500 °C, keeping other processing parameters same as mentioned above.

Characterization using XRD, Raman spectroscopy and electron microscopy

X-ray diffraction (XRD) studies on the SPS sintered and powder specimens were conducted using an X-Ray Diffractmeter (*Rigaku MiniFlexII*). The powder samples were pressed on a hydraulic press in the form of circular pallets (~10 mm dia) for this study. Morphology and chemical composition of powder and SPS sintered samples were investigated on a Field Emission Scanning Electron Microscope (*FE-SEM; LEO 440*) with *Oxford ISIS 300* energy dispersive spectroscopy (EDS) attachment. The SPS sintered samples were electropolished for microscopic observations. Raman spectroscopy measurements were performed on a Macro Raman *Renishaw inVia* system with 514 nm laser. Vickers microhardness of SPS sintered specimens was measured on a microhardness tester (*Future Tech Corp*) at the load of 200 g. Transmission electron microscopy (TEM) of powder samples was performed on specially prepared TEM grid. Whereas, SPSed specimens were extracted to 3 mm disc (~0.5 mm thick) on a diamond saw followed by polishing up to ~100 mm thickness and subsequent ion beam milling to perforation at center for the TEM study on a *FEI Technai G2 F30 STWIN microscope*.

Results and discussion

Phase analysis using X-ray diffraction

XRD patterns of Al-0.5 Gr powder specimen and SPS sintered at 450, 500, and 550 °C are shown in **Fig. 1**. The powder sample depicted predominant aluminium phase and oxide phase in traces (**Fig. 1(a)**) suggesting high quality of chemical synthesis approach followed. XRD patterns of SPS sintered solid specimens (pure Al, Al-0.5 Gr, Al-2 Gr, Al-4 Gr, and Al-6 Gr, sintered at 500 °C) are shown in **Fig. 1(b-d)**.

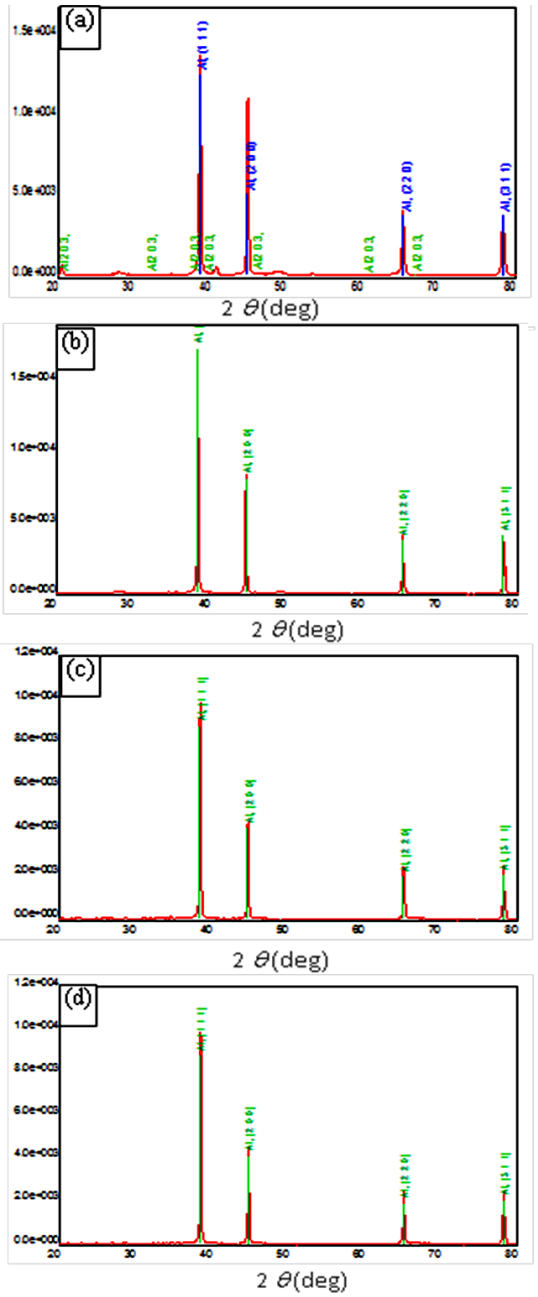

Fig. 1. XRD patterns of (a) Al-0.5 Gr and SPS sintered powder at the temperatures of (b) 450 °C, (c) 500 °C, and (d) 550 °C.

The XRD plots depict single phase aluminium matrix suggesting any traces of oxides formed during *in-situ* chemical synthesis of Al-Gr powder samples were eliminated during SPS sintering. The (002) reduced graphene (Gr) peak is usually observed at ~27° **[4, 7, 15]** which, however, was suppressed in all the Al-Gr sintered specimens. It is evident that reduced graphene (Gr) formed during *in-situ* chemical synthesis processing has been few layer/few hundred nanometer thick even for the maximized GO content, *i.e.* for the Al-6 Gr sample and could not be detected by the XRD detector. Similar observations are reported by Pavithra *et al* **[9]** for PRED electrodeposited Cu-Gr nanocomposite foils.

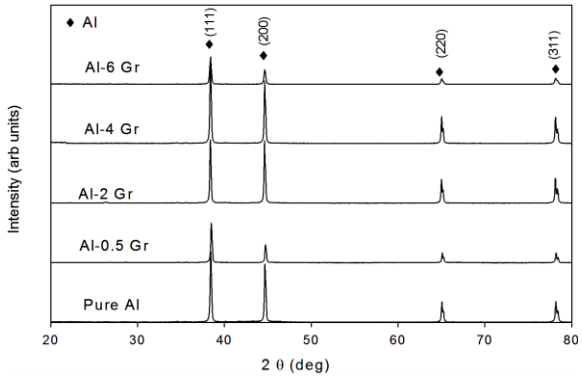

Fig. 2. XRD patters of aluminium-reduced graphene (Al-Gr) nanocomposites sintered at 500 °C using SPS.

Microstructure and chemical analysis using electron microscopy

Fig. 3 shows SEM micrographs and corresponding EDS patterns for Al-Gr nanocomposite powders synthesized using the *in-situ* chemical synthesis method. Two different powder compositions (*i.e.* Al-2 Gr, and Al-6 Gr) were chosen and respective SEM micrographs and EDS spectra are depicted in **Fig. 3(a-c)** and **Fig. 3(d-f)**. The as-received aluminium powder was found having irregular morphology with average particle size as ~40 mm. Cryomilling in liquid nitrogen medium resulted in flattening and coarsening of particles, however, crystallite size (calculated by XRD patterns using the Williamson-Hall method **[16]** was found reduced to 21.7 nm as compared to 44.8 nm (in the as received condition).

Fig. 3(a) shows low magnification SEM micrograph of Al-2Gr powder depicting coarse and flattened particles usually below 100 µm size. At higher magnification a coarse aluminium powder without any chemical structure is observed (**Fig. 3(b)**). The *in-situ* chemical synthesis method adopted in this work is expected to produce sheet-like **[4, 9]**/wrinkled **[3]** structure typical of reduced graphene oxide (GO) and has been referred as reduced graphene (Gr). The corresponding EDS spectra (shown in **Fig. 3(c)**) depicts predominantly aluminium peak with minor contents of C and O. The absence of any chemical structure over aluminium particles and a predominant Al peak through EDS profile suggests that the GO concentration has been insufficient to enable achieving coating of reduced

graphene over aluminium particles. **Fig. 3(d)** shows a low magnification SEM image of Al-6 Gr powder depicting structure and morphology similar to that in **Fig. 3(a)**. The high magnification SEM image of the Al-6 Gr powder shown in **Fig. 3(e)** depicts wrinkled structure that is typical of reduced graphene (Gr) **[3, 9]**. The wrinkled structure fully covers the aluminium particles, suggesting GO concentration is adequate to achieve uniform layer of reduced graphene over aluminium particles.

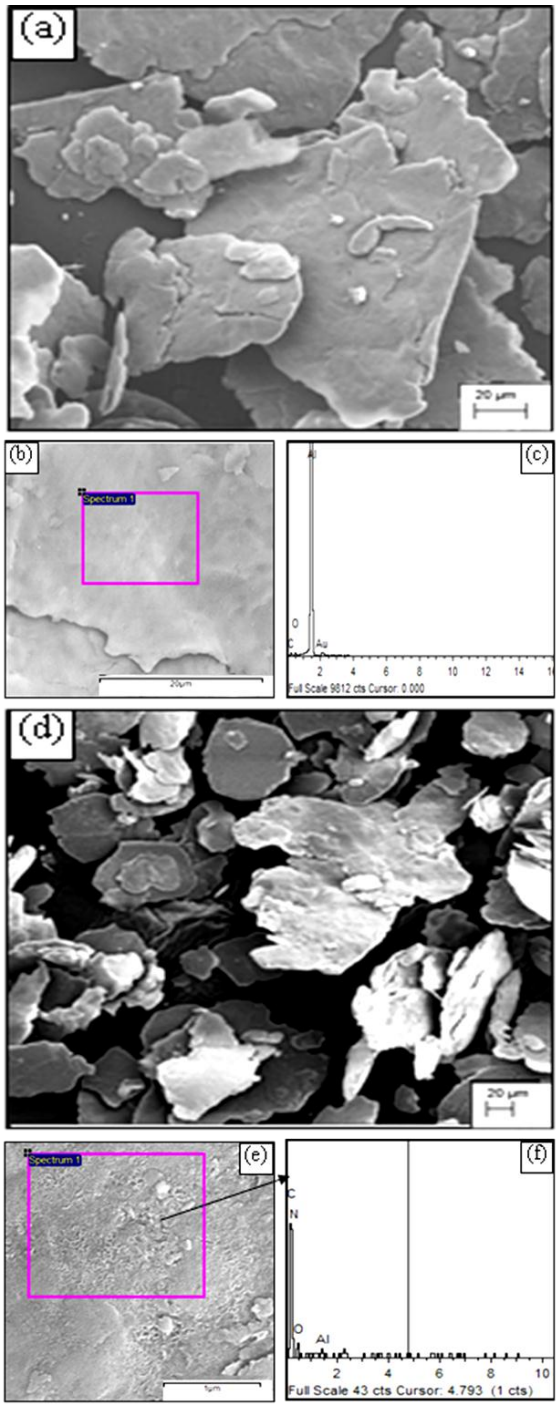

Fig. 3. SEM micrographs of *in-situ* synthesized nanocomposite powders (a) Al-2 Gr at low mag., (b) Al-2 Gr at high mag., (d) Al-6 Gr at low mag. Corresponding EDS spectra of Al-2 Gr powder (e) depicts predominantly aluminium (Al) peak and EDS spectra of Al-6 Gr powder (f) depicts predominantly carbon (C) peak.

However, thickness of reduced graphene is predicted to be only few layers since it could not be detected in the XRD results (**Fig. 2**). The corresponding EDS pattern (**Fig. 3(f)**) clearly shows predominance of carbon (C) and minor O and Al content that infers Al particles are fully covered with graphene derived carbon and confirms uniform dispersion of graphene in the aluminium matrix. The minor content of nitrogen (N) was observed for both Al-2 Gr and Al-6 Gr samples that was due to alloying with nitrogen at the cryomilling stage.

Fig. 4 shows TEM micrographs of Al-6 Gr powder and SPS sintered material. **Fig. 4(a)** is the bright field TEM image of Al-6 Gr powder sample showing wrinkles in the size of 100 nm or more. The well-defined electron diffraction pattern (SADP) depicts bright spots due to regular hexagonal lattice of crystalline graphene (encircled in **Fig. 4(a)**) and adjacent spots due to polycrystalline aluminium. **Fig. 4(b)** is the bright field TEM image of SPS sintered Al-6 Gr sample that shows aluminium grains with graphene wrinkles at triple junctions (shown by arrow). The corresponding SADP pattern shown in the same figure depicts diffraction spots of graphene which are diffused, since, diffraction pattern due to the aluminium matrix is more dominant. These TEM images suggest presence of reduced graphene as thin interlayers at the grain boundaries of the aluminium matrix.

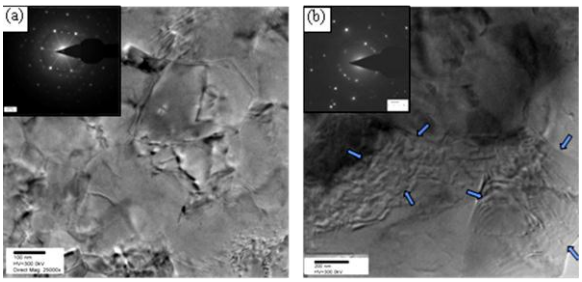

Fig. 4. TEM micrograph of (a) *in-situ* synthesized Al-6 powder depicting graphene wrinkles with SADP pattern and (b) SPS sintered Al-6 Gr with corresponding SADP pattern.

Spectroscopic analysis using Raman spectroscopy

Fig. 5 shows Raman spectra of *in-situ* synthesized Al-Gr powders: (a) Al-2 Gr, (b) Al-4 Gr, and (c) Al-6 Gr. The same figure also shows Raman spectra of SPS sintered Al-6 Gr sample in **Fig. 5(d)**, which was generated at electropolished cross-sectional surface of the sample. The D, G, 2D, and D+G bands are observed at the wavenumber of ~1348 cm^{-1}, ~1597 cm^{-1}, ~2690 cm^{-1}, and 2930 cm^{-1}. Among various bands observed, the prominent bands are D and G for the powder samples (**Fig. 5(a-c)**) and confirm the presence of graphene derived carbon materials. These findings are in agreement with the studies conducted on GNS-Al nanocomposites **[3]**, electropolished and annealed Cu-Gr foils **[9]**, RGO-Cu nanocomposites **[10]**, Graphene [**17]** etc. The I_D/I_G ratio for the three powder samples is progressively decreased and found

as 1.46, 1.42, and 1.20 for Al-2 Gr, Al-4 Gr, and Al-6 Gr, respectively. Moreover, intensity of both the peaks progressively decreased with increasing "addition of GO/presence of reduced graphene". This behavior is likely due to the doping in the graphene honeycomb structure, that is responsible for local defects and disorder, thereby creating an effective change in the E_{2g} photon corresponding to the sp^2 atoms (G band) and k-point photon of A_{1g} symmetry (D band) **[4, 18]**. An additional observation from **Fig. 5** for the powder samples is that Raman shift peaks are observed at the wavenumber ~2690 (2D) and ~2930 (D-G). The 2D band is a characteristic band that represents the number of layers/thickness of graphene **[17, 19]**. Usually, single layer graphene depicts a sharp 2D peak with its intensity four times more than the G peak. Whereas, a modulated bump indicates multi-layered graphene has been synthesized **[17, 20]**.

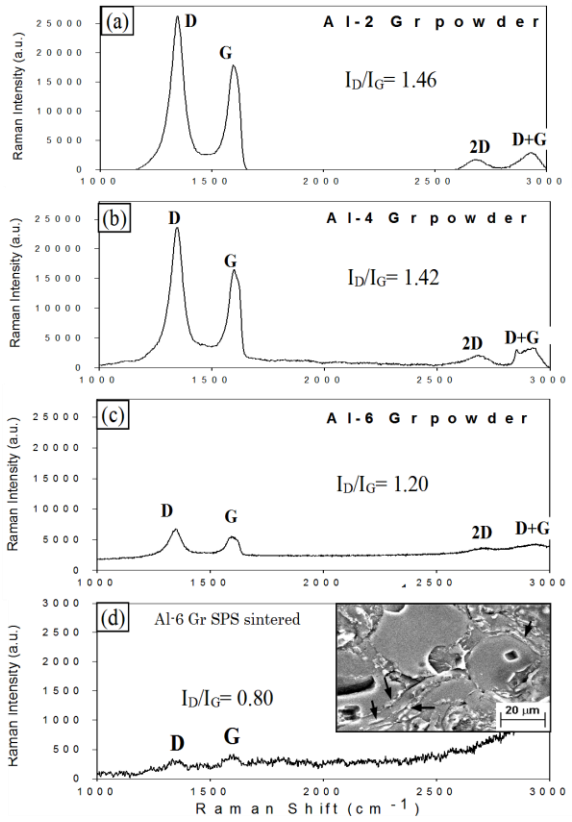

Fig. 5. Raman spectra of Al-Gr nanocomposites: (a) Al-2 Gr powder, (b) Al-4 Gr powder, (c) Al-6-Gr, and (d) Al-6 Gr SPS sintered showing D, G, 2D, and D+G bands at the wavenumber of 1348 cm^{-1}, ~1597 cm^{-1}, ~2690 cm^{-1}, and 2930 cm^{-1}. The inset in figure 5(d) shows cross-sectional SEM micrograph of electropolished Al-6 Gr SPSed sample.

The present work shows modulated peak for all the Al-Gr powder samples (**Fig. 5(a-c)**) with intensity of 2D band significantly lower than the G peak illustrating multi-layered graphene has been synthesized. The intensity of the 2D peak is abysmally small for the Al-6 Gr powder sample, indicating a multilayered graphene product is formed that is also depicted by the SEM micrograph show in **Fig. 3(e)**. The Raman spectra (**Fig. 5(d)**) for the SPS sintered Al-6 Gr sample also shows presence of D and G bands confirming the presence of graphene derived carbon in the SPS sintered nanocomposite. However, the I_D/I_G ratio is significantly small (~0.80), which is the results of a weak Raman pattern acquired due to the presence of thin graphene interlayers in the coarse grained matrix of pure aluminium. The electropolished cross-sectional SEM image of the specimen (shown in the inset in **Fig. 5(d)**) suggests that graphene is present as thin interlayers at the grain boundaries (indicated by arrows). The EDS spectra analysis of the SEM image shown in **Fig. 5(d)** revealed chemical composition as: C: 9.28; N: 0.76; O: 8.07, and Al: 78.27 by wt%, confirming the presence of graphene derived carbon that is available as the interlayers at the grain boundaries.

Mechanical behaviour after SPS sintering

Vickers microhardness of Al-Gr nanocomposites at different parameters of spark plasma sintering (SPS) was measured. The microhardness of cryomilled pure Al was found as 40±2 HV_{200}, which was found enhanced and progressively increased with the content of reduced graphene. For the Al-0.5 Gr sample, the microhardness at different SPS temperatures of 450, 500, and 550 °C was measured and found maximum as 42±4 at 500 °C. For the various Al-Gr nanocomposites *i.e.*, Al-0.5 Gr, Al-2 Gr, Al-4 Gr, and Al-6 Gr, microhardness at the SPS sintering temperature of 500 °C was measured as 42±4, 52±3, 55±4, and 63±4 HV_{200}, respectively. Hence, with increasing graphene oxide (GO) as the precursor (*i.e.*, with GO content as 0.5, 2, 4, and 6 ml in 10 g Al), Vickers microhardness was found progressively increased due to increased content of reduced graphene, which has been confirmed by the SEM studies (refer **Fig. 3** for Al-2 Gr and Al-6 Gr samples). At the optimized SPS temperature of 500 °C, the increase in the microhardness values is calculated as 5%, 30%, 38%, and 58% for the Al-0.5 Gr, Al-2 Gr, Al-4 Gr, and Al-6 Gr samples, respectively, as compared to pure aluminium. For the graphene nanosheets (GNSs)/Al nanocomposites synthesized by flake powder metallurgy method, Wang *et al* **[3]** have reported 62% improvement in tensile strength (with 0.3 wt% addition of GNSs) as compared to unreinforced pure aluminium matrix. Similarly, for PRED electrodeposited copper-graphene (Cu-Gr) foils, Pavithra *et al* **[9]** have reported 96% improvement in hardness as compared to pure copper. Assuming the constrained factor of 3 for metallic materials **[21]**, the calculated tensile strength values for pure Al, Al-0.5 Gr, Al-2 Gr, Al-4 Gr, and Al-6 Gr samples of the present study are 133±7, 140±2, 173±10, 183±13, and 210±13 MPa, respectively, suggesting about 58% improvement in tensile strength for the maximized GO content (*i.e.* for the Al-6 Gr sample).

Conclusion

Aluminium-graphene (Al-Gr) nanocomposites with varying compositions have been synthesized by a novel *in-situ* chemical synthesis method using graphene oxide (GO) as the precursor. These nanocomposite powders have been subsequently sintered using spark plasma sintering (SPS) under optimized conditions. Graphene oxide (GO) is reduced to graphene (Gr) during chemical synthesis. A homogenous dispersion of graphene in the aluminium matrix is achieved for the maximized GO content, indicated by a uniform few layer thickness of reduced graphene over aluminium particles for Al-6 Gr powder specimen, which is revealed by the SEM analysis. The TEM examination has suggested graphene structure composed of wrinkles of 100 nm or more in size. The crystalline nature of graphene is depicted by the SADP diffraction pattern resembling with regular hexagonal lattice of crystalline graphene. Synthesis of multilayered graphene has been confirmed by Raman spectroscopy for varying content of GO in the aluminium matrix. The SPS sintered nanocomposites have revealed presence of reduced graphene as thin interlayers at the grain boundaries through electron microscopic studies. Vickers microhardness is found increased with increased content of reduced graphene. For the maximized GO content in the present study has delivered an increase of 58% in the microhardness as compared to pure aluminium.

Acknowledgements

This research work has been carried out with the financial support by CSIR-NPL, which is gratefully acknowledged. One of the author (Anil Kumar) received grant under post-doctoral fellowship research at NPL. The authors acknowledge Dr. S.R. Dhakate, Head-Physics and Engineering of Carbon group for arranging Raman Spectroscopy; Mr. M. Sarvanan, Mr. Naval Kishore Upadhyaya, and Mr. Dinesh Singh for taking the SEM, XRD and TEM measurements, respectively.

References

1. Randviir, E. P.; Brownson, D. A. C.; Banks, C. E.; *Mater. Today*, **2014**, *17*, 426.
2. Shin, S. E.; Bae, D. H.; *Composites: Part A*, **2015**, *78*, 42.
3. Wang. J.; Li, Z.; Fan, G.; Pan, H.; Chen, Z.; Zhang, D.; *Scripta Mater.*, **2012**, *66*, 594.
4. Kumar, A.; Husale, S.; Srivastava, A. K.; Dutta, P. K.; Dhar, A.; *Nanoscale*, **2014**, *6*, 8192.
5. Lu, G.; Yu, K.; Wen, Z.; Chen, J.; *Nanoscale*, **2013**, *5*, 1353.
6. Wang, X.; Zhou, X.; Yao, K.; Zhang, J.; Liu, Z.; *Carbon*, **2011**, *49*, 133.
7. Zhang, C.; Peng, X.; Guo, Z.; Cai, C.; Chen, Z.; Wexler, D.; Li, S.; Liu, H.; *Carbon*, **2012**, *50*, 1897.
8. Jiang, L.; Li, Z. Q.; Fan, G. L.; Zhang, D.; *Scripta Mater.*, **2011**, *65*, 412.
9. Pavitra, C. L. P.; Sarada, B. V.; Rajulpati, K. V.; Rao, T. N.; Sundararajan, G.; *Sci. Rep.*, **2014**, *4*, 4049.
10. Hwang, J.; Yoon, T.; Jin, S. H.; Lee, J.; Kim, T. S.; Hong, S. H.; Jeon, S.; *Adv. Mater.*, **2013**, *25*, 6724.
11. Jun, H. L.; Xin, W. Y.; Guo, T. J.; Min, W. H.; Bin, W. H.; Xiu, Q. J.; Yao, W.; Xian, L. J.; Quan, L. J.; *Int J. Electrochem. Sci.*, **2012**, *7*, 11068.
12. Chang, C. W.; Hon, M. H.; Leu, L. C.; *ECS J. Solid State Sci. Technol.*, **2015**, *4*, M18.
13. Tiwari A. (Eds.); Graphene Materials; John Wiley and Sons: USA, **2015**.
14. Kote, L. J.; Kim, J.; Zhang, Z.; Sun, C.; Huang, J.; *Soft Matter*, **2010**, *6*, 6096.
15. Xu, Y. X.; Sheng, K. X.; Li, C.; Shi, G. Q.; *ACS Nano*, **2010**, *4*, 4324.
16. Williamson, G. K.; Hall, W. H.; *Acta Metall.*, **1953**, *1*, 22.
17. Wall, M.; Thermo Scientific Application Note: 52252, **2011**.
18. Karim, M. R.; Shinoda, H.; Nakai, M.; Hatakeyama, K.; Kamihata, H.; Matsui, T.; Taniguchi, T.; Koinuma, M.; Kuroiwa, K.; Kurmoo, M.; Matsumoto, Y.; Hayami, S.; *Adv. Funct. Mater.*, **2013**, *23*, 323.
19. Ferrari, A. C.; Meyer, J. C.; Scardaci, V.; Casiraghi, C.; Lazzeri, M.; Mauri, F.; Pissanec, S.; Jiang, D.; Novoselov, K. S.; Roth, S.; Geim, A. K.; *Phy. Review. Letter.*, **2006**, *97*, 187401.
20. Gupta, T. K.; Singh, B. P.; Tripathi, R. K.; Dhakate, S. R.; Singh, V. N.; Panwar, O. S.; Mathur, R. B.; *RSC Advances*, **2015**, *5*, 16921.
21. Dieter, G. E. (Eds.); Chapter 9, Mechanical Metallurgy; McGraw-Hill Book Co.: UK, **1988**.

